ISSN 0027-1349, Moscow University Physics Bulletin, 2015, Vol. 70, No. 5, pp. 382–389. © Allerton Press, Inc., 2015.
Original Russian Text © S.A. Magnitskiy, P.P. Gostev, D.N. Frolovtsev, V.V. Firsov, 2015, published in Vestnik Moskovskogo Universiteta. Fizika, 2015, No. 5, pp. 53–60.

OPTICS AND SPECTROSCOPY. LASER PHYSICS

Characterization of Polarization-Angular Spectrum of Type-I SPDC in BBO Crystal

S. A. Magnitskiy, P. P. Gostev, D. N. Frolovtsev, and V. V. Firsov

Department of Physics, International Laser Center, M.V. Lomonosov Moscow State University, Moscow, 119991 Russia

e-mail: sergeymagnitskiy@gmail.com

Received May 20, 2015; in final form, June 26, 2015

Abstract—We analyze the state of type-I SPDC polarization in nonlinear uniaxial crystals using a coordinate system connected with a pump beam. The entanglement loss due to the Migdall effect is examined. The analytical expressions for polarization components of the signal and idler waves for the frequency-degenerate regime are obtained. The numerical results for BBO crystal are also adduced.

Keywords: polarization, spontaneous parametric down-conversion, non-collinear interaction, quantum state.

DOI: 10.3103/S0027134915050094

1. INTRODUCTION

Spontaneous parametric down-conversion of light (SPDC) is one of the most striking physical effects [1–5] used currently for obtaining correlated and entangled photons [6–8]. The unusual properties of such photons open the way for solving the problems of quantum cryptography [9, 10], teleportation [11–13], dense coding [14] and quantum computations [11] as well as being the subject of the unflagging interest in basic research [15, 16]. The increasing complexity of the tasks, facing researchers, causes the need for developing SPDC sources of improved quality. This motivated scientists [17], engaged in the development of SPDC sources, to take into account more subtle features of SPDC [18]. One of these features is the dependence of SPDC polarization on its propagation direction inside a nonlinear crystal. Despite the fact that this effect is quite obvious from the point of view of classical electrodynamics, its role in generation of entangled photons was noted for the first time only in 1997 [19]. The first experimental observation was demonstrated in 2011 [20]. But so far authors working with non-collinear SPDC [6, 21, 22] usually considered the polarization of output radiation as strictly horizontal or vertical without taking into account the direction of wave propagation. The impact of this effect on the entanglement of generated biphotons states being insignificant for a single-crystal schemes becomes essential in more complex systems such as double-crystal SPDC schemes [6] as well as in periodic and aperiodic nonlinear photonic crystals [23]. In particular, this effect, which is sometimes called the Migdall effect [20] in the literature on quantum optics, needs to be considered in the design of high-efficiency SPDC generators of polarization entangled photons. This paper analyzes the polarization-angular spectrum of SPDC in uniaxial negative crystals in the conditions of type-I phase matching. We also touch briefly on the impact of the Migdall effect on the degree of entanglement of biphoton states produced in crossed-crystal type-I configuration.

2. POLARIZATION PROPERTIES OF PHOTONS GENERATED VIA FREQUENCY-DEGENERATE TYPE-I SPDC

It is known that parametric generation [24] is seeded by zero-point fluctuations of electromagnetic vacuum which can be directly measured, for example, in the process of injected parametric amplification [25]. Type-I SPDC radiation propagates over the surface of a cone [6, 11] with a cone angle equal to an angle α of non-collinearity. In our study we used the Newlight Photonics 3-mm-thick BBO crystal cut for the type-I *e–oo* non-collinear degenerate interaction, as a prototype for generation of correlated photon pairs [26]. Figure 2 shows the spatial distribution of SPDC radiation from this crystal when pumping by 70-mW 532-nm cw laser.

The spatial structure was recorded by the CCD camera mounted perpendicular to the pump beam. A narrow-band interference filter ($\Delta\lambda \sim 8$ nm) at 1.064 microns was installed in front of the camera.

For mathematical analysis of SPDC polarization it is possible to choose a coordinate system in different ways. One can bind the coordinate system either to the pump beam (“pump basis”), or to the scattered beam

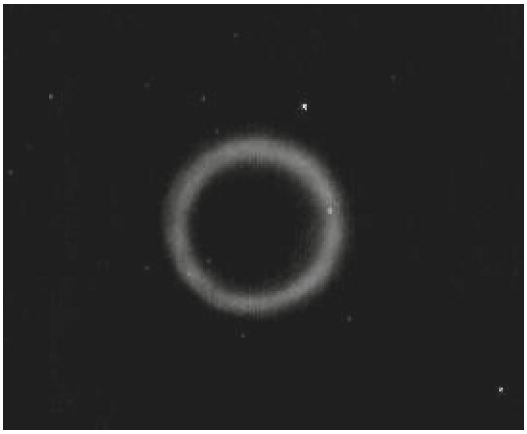

Fig. 1. The spatial structure of non-collinear type-I SPDC radiation from BBO crystal.

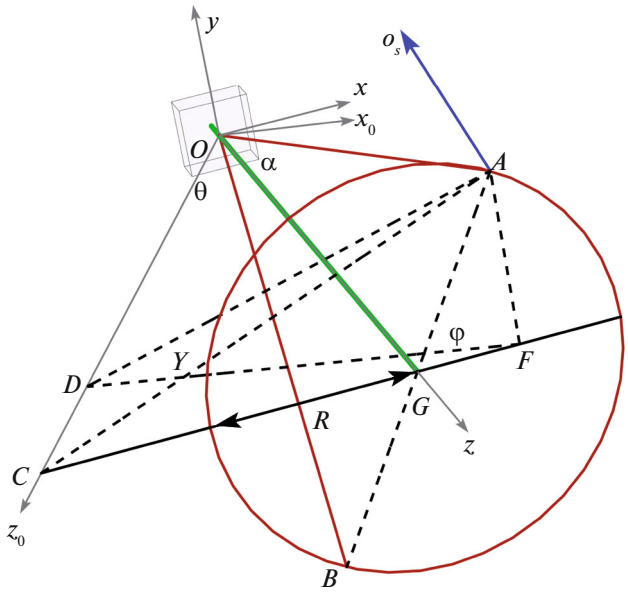

Fig. 2. Geometry of non-collinear parametric interaction in the conditions of type-I phase-matching. *OA* and *OB* are the beams of the signal and idler modes, o_s is the polarization vector of the signal wave; *OG* is the pump beam. *OC* is the optic axis of the crystal and *D* is the projection of point *A* on the crystal axis. The labeled angles shown are *AGF*(φ), *ADF*(γ), non-collinearity angle *AOG*(α) and crystallographic angle *GOC*(θ).

("natural basis"). In particular, in previously mentioned works [19, 20] the polarization for each SPDC beam direction $\mathbf{n}_{\text{SPDC}}$ was considered in its own natural basis, the *x* axis was directed along the beam and the *y* axis was chosen perpendicular to the beam in the plane, which was perpendicular to the principal plane of the pump beam. In our analysis we have used a pump basis, general for all beams. Let a linearly polarized pump beam falls along the normal to a nonlinear uniaxial crystal that is cut under the first type of phase-matching. We choose the *z* axis of the Cartesian coordinates (see Fig. 2) in the direction of the unit vector $\mathbf{n}_p$ along the pump beam.

The *x* axis is chosen in the principal plane of the pump beam, i.e. in the plane that passes through the pump beam and the optical axis *OC* of the crystal which forms an angle θ with $\mathbf{n}_p$. Below, we will refer to this plane as horizontal. In the pump basis the polarization of the pump $\mathbf{e}_p$ can be written as $\mathbf{e}_p = \{1, 0, 0\}$. The lack of *z*-components of polarization reflects the transversality of the pump wave. Naturally, the polarization vector of SPDC radiation in this basis has all three components. Both waves of the SPDC have the same frequency in the degenerate mode and, therefore, the difference in the terms of the "signal" ($\frac{\omega_p}{2} \leqslant \omega_s < \omega_p$) and "idler" ($0 < \omega_i \leqslant \frac{\omega_p}{2}$) waves as waves with different frequencies disappears. Further, we will call a beam, propagating at the angle φ in the range from 0 to π a signal wave and a beam "paired" to it ($\pi \leqslant \varphi < 2\pi$) an idler wave.

The phase-matching conditions i.e. the conditions of conservation of energy and momentum, which should be carried out simultaneously, are as follows:

$$\begin{cases} \omega_p = \omega_s + \omega_i \\ \mathbf{k}_p = \mathbf{k}_s + \mathbf{k}_i \end{cases} \qquad (1)$$

where the index *p* denotes the characteristics of pumping and the indexes *s* and *i* refer to signal and idler modes, respectively. SPDC beams of equal frequencies form a circle of radius *R* in the (*x*, *y*) plane [3, 6]. It is convenient to describe every point of this circle with the polar angle φ which shows the position of a point with respect to the horizontal plane. We will count off the angle φ counterclockwise from this plane. The conservation laws impose restrictions on the spatial position of the bound SPDC modes, viz., if the signal mode is characterized by the polar angle φ_s, then the idler mode of a biphoton field will be described by the angle $\varphi_i = \varphi_s + \pi$. In type-I SPDC the pump wave is an extraordinary *e*-wave, while the signal and idler waves are ordinary *o*-waves.

As is known [27], in a uniaxial crystal the polarization of the *o*-wave is normal to the principal plane and the polarization of the pump wave lies in the extraordinary direction. Also note that the ray vector for the ordinary wave is parallel to the wave vector. In Fig. 2, the polarization of the *o*-wave is perpendicular to the plane *OAC* for a beam that is characterized by the angle φ. Since the slope of this plane varies with the angle φ, the polarization vector changes its direction in space when this angle changes.

Let us consider an arbitrary SPDC beam which is characterized by some φ. This beam passes through the point *A* (see Fig. 1) and the corresponding idler beam passes through the point *B*. As noted above, the

polarization vector of the signal wave should be orthogonal to the *OAC* plane. The position of the *OAC* plane to the horizontal plane will be characterized by the angle γ which will determine the inclination of the polarization vector. The angle γ is formed by the lines *AD* and *FD*, which are perpendicular to the crystal axis. At the first step it is convenient to introduce the auxiliary coordinate system (x_0, y_0, z_0) which is associated with the optic axis of the crystal.

The z_0 axis is directed along the optical axis of the crystal *OC* and the x_0 axis is placed in the horizontal plane *OGC*, in which the *x* axis is chosen. In this coordinate system the polarization vector is given by:

$$o_{s,0}(\gamma) = \{-\sin\gamma, \cos\gamma, 0\}. \quad (2)$$

This follows directly from Fig. 2. In fact, the angle γ lies in a plane that is perpendicular to the axis of the crystal *OC* and the vector $\mathbf{o}_{s,0}$ is perpendicular to the *OAD* plane. Therefore, the vector $\mathbf{o}_{s,0}$ lies in the plane of the angle γ and is inclined to the vertical plane under the same angle γ.

The expression for the vector $\mathbf{o}_s$ in the reference system (x, y, z) can be obtained by multiplying expression (2) by the rotation matrix $R_y(\theta)$ around the vertical axis $y_0 = y$ at the angle θ in a clockwise direction:

$$R_y(\theta) = \begin{pmatrix} \cos\theta & 0 & -\sin\theta \\ 0 & 1 & 0 \\ \sin\theta & 0 & \cos\theta \end{pmatrix}. \quad (3)$$

After turning the system (x, y, z), the polarization vector will be:

$$\mathbf{o}_s(\gamma,\theta) = R_y(\theta)\mathbf{o}_{s,0}(\gamma) = \{-\sin\gamma\cos\theta, \cos\gamma, -\sin\gamma\sin\theta\}. \quad (4)$$

To obtain the final formula, it is necessary to derive an explicit expression for the angle γ as a function of the angles φ, α, and θ, that can be done directly from the stereometric relationships of the scheme shown in Fig. 2. Let us restore the perpendicular *AD* from the point *A* to the axis of the crystal *OC* and the second perpendicular *AF* to the continuation of the *CG* line, which lies in the horizontal plane and passes through the center of the circle *G*. In this notations $\tan\gamma = AF/FD$, where $AF = R\sin\varphi = OG\tan\alpha\sin\varphi$. To calculate *FD*, note that *FD* is the leg of a right triangle *FDC* and the angle *DFC* is equal to the angle θ because it is formed by the lines *FD* and *FC*, which are perpendicular to the lines *OC* and *OG*, respectively. Then, $FD = FC\cos\theta = (FG + GC)\cos\theta = (OG\tan\alpha\cos\varphi + OG\tan\theta)\cos\theta$. Using these expressions for *AF* and *FD* we find:

$$\tan\gamma = \frac{AF}{FD} = \frac{\tan\alpha\sin\varphi}{(\tan\alpha\cos\varphi + \tan\theta)\cos\theta}. \quad (5)$$

When deriving the expression (5), we have tacitly assumed that $0 \leqslant \varphi \leqslant \pi/2$. However, since $\cos\varphi$ and, as a result, *FG* change their signs at $\varphi = \pi/2$, then both geometries are equivalent. Therefore, the expression (5) retains its form for all angles $\varphi > \pi/2$.

Thus, the polarization vector of SPDC wave at $0 \leqslant \varphi \leqslant \pi$ has the following components in the pump basis:

$$\mathbf{o}_s(\varphi,\alpha,\theta) = \{-\sin\gamma\cos\theta, \cos\gamma, -\sin\gamma\sin\theta\}, \quad (6)$$

where

$$\gamma = \arctan\left(\frac{\tan\alpha\sin\varphi}{(\tan\alpha\cos\varphi + \tan\theta)\cos\theta}\right). \quad (7)$$

We would like to make some clarification concerning the polarization vector $\mathbf{o}_s$. In our consideration we are interested only in the directions of the electromagnetic field of the signal and idler SPDC waves and are not interested in its phase. The vector $\mathbf{o}_s$ should not be identified with electric field strength. It was introduced only for the convenience of description and could be chosen with equal success as it is represented in Fig. 2, and in the opposite direction. We agreed to choose this vector, both for the signal and the idler waves, in such a way that its *y*-component was positive at all angles φ. The vector $\mathbf{o}_i(\pi \leqslant \varphi \leqslant 2\pi)$ according to this choice is:

$$\mathbf{o}_i(\varphi,\alpha,\theta) = \{\sin\gamma\cos\theta, \cos\gamma, \sin\gamma\sin\theta\}, \quad (8)$$

where the angle γ is determined by expression (7), while replacing φ with $2\pi - \varphi$. This is clear from symmetry of the problem.

Indeed, in a mirror image relative to the *OCG* plane the vector $\mathbf{o}_s(\varphi \leqslant \pi)$ transforms into the vector $\mathbf{o}'_s$, which is parallel to the vector $\mathbf{o}_i(2\pi - \varphi)$, but is aimed in the opposite direction with respect to our choice of the sign of the *y*-component. Its components are connected with the components of the vector o_s as follows: $\mathbf{o}'_s = \{o_{s,x}, -o_{s,y}, o_{s,z}\}$. Then, to obtain the vector $\mathbf{o}_i(\pi \leqslant \varphi \leqslant 2\pi)$ it is sufficient to invert this vector, i.e., to change the signs of all its components, that will lead to formula (8). As can be seen from (7) the polarization vector of the signal wave at $\varphi = 0$ and $\varphi = \pi$ has only *y*-component i.e., it is strictly perpendicular to the horizontal plane. This also follows directly from Fig. 2. At all other angles the polarization vector has other components, which reach the maximum values at the angles γ at which the OAC plane touches the surface of the SPDC cone. It is also easy to see that the polarization vector $\mathbf{o}_s$ turns around the z_0 axis in the positive direction of a right-handed screw with an increase of the angle φ and always remains perpendicular to the z_0 axis in the *AFD* plane.

3. THE RESULTS OF NUMERICAL CALCULATIONS OF SPDC POLARIZATION FOR BBO CRYSTAL

This section presents the results of numerical calculations of the vector components $\mathbf{o}_s(\varphi, \alpha, \theta)$ and

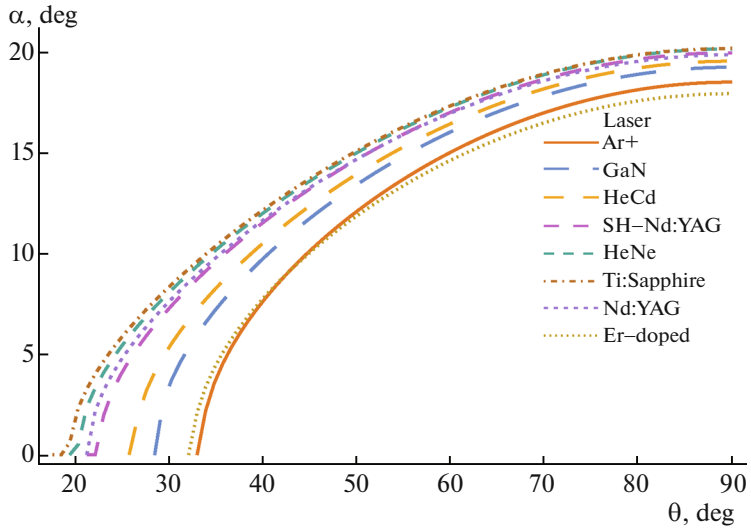

Fig. 3. Dependences of non-collinearity angle α on crystallographic angle θ for some types of lasers in the visible and near infrared ranges: Ar^+ (350 nm), GaN (405 nm), HeCd (441.6 nm), second harmonic of Nd^{3+}:YAG (532 nm), HeNe (632.8 nm), Ti:Sapphire (800 nm), Nd^{3+}:YAG (1064 nm), Er-doped (1550 nm). Calculations are made for frequency-degenerate modes.

$\mathbf{o}_i(\varphi, \alpha, \theta)$ for BBO crystal according to the expressions (6) and (7). The choice of this crystal is caused by the fact that it is one of the most popular crystals in quantum optics used for generation of correlated and entangled photons.

The approximate Selmeier's formulas [28] were used in the approximation up to λ^2 to calculate the refraction indices n_e and n_o:

$$n_o^2 = 2.7359 + \frac{0.01878}{\lambda^2 - 0.01822} - 0.01354\lambda^2,$$
$$n_e^2 = 2.3753 + \frac{0.01224}{\lambda^2 - 0.01667} - 0.01516\lambda^2. \quad (9)$$

As seen from (6) and (7) the angle γ, and therefore, a rotation angle of the polarization vector, depends on the angle of the non-collinearity α and phase-matching angle θ. When α is greater and θ is smaller the effect is stronger. The angles α and θ are not independent parameters and are connected through phase-matching conditions and the dispersion relationship (9). The dependencies of the non-collinearity angle α on the angle θ for BBO crystal in the degenerate mode with various wavelengths of the pump, which are typical for the most commonly used lasers, are given in Fig. 3.

It is seen from the calculated dependencies that for different wavelengths different combinations of the angles α and θ are realized, which in turn determine the value of a rotation angle of a SPDC polarization vector.

Figures 4 and 5 show the calculated values of the vector components of SPDC polarization in the BBO crystal for two cases: for the crystal that is used in our laboratory (α = 1.8° and θ = 23.3°) with 532-nm pumping (Fig. 4) and for a crystal (α = 13.6° and θ = 45°) with λ_p = 800 nm (Fig. 5).

We note that the angle α is the non-collinearity angle inside the crystal as it is defined in Fig. 2. The external non-collinearity angle α_{ext} will be, naturally, greater and can be calculated using Snell's law. Thus, for the crystal used in our laboratory $\alpha_{ext} = 3°$. The calculated parameters that correspond to Fig. 4 are chosen for practical reasons. As for the parameters corresponding to Fig. 5 they were selected for the following reasons: first, the wavelength λ_p corresponds to the wavelength of the widespread sapphire titanate laser; second, for these conditions manifestation of polarization rotation in BBO crystal reaches its maximal value. This follows from the fact that the angle γ that determines the values of *x*-components of polarization has its maximum for these parameters wherein the curves for the *x*- and the *z*-components are the same.

The resulting curves show the following regularities: with increasing the angle φ from 0 to π a horizontal component of the vector s increases, reaches a maximum at a certain angle φ, then decreases monotonically and at φ = π the polarization becomes vertical again.

One more feature is that for each value of the angle φ there is a certain angle φ* at which a polarization vector at an angle φ coincides with a polarization vector at an angle φ*. In Fig. 2, this corresponds to the fact that the *OCA* plane crosses the circle *R* at two points. This occurs at all angles φ, except one when this plane touches the surface of the cone. In this case, the "twin-vector" coincides with the original one.

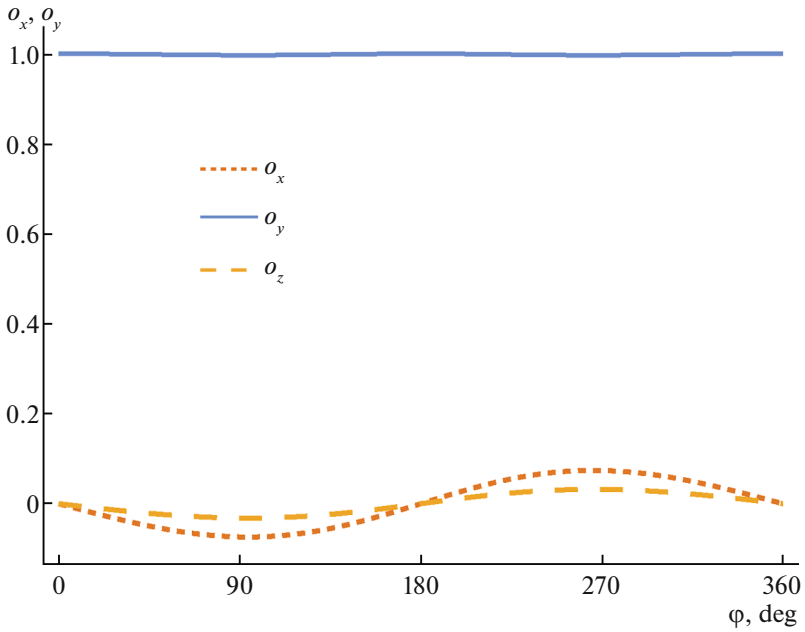

Fig. 4. The projections of the polarization vector $\mathbf{o}_s(\varphi, \alpha, \theta)$ in BBO crystal as a function of the polar angle φ, calculated in the pump basis. Calculations were made for non-collinear ($\alpha = 1.8°$) frequency-degenerate regime with 532-nm pump ($\theta = 23.3°$).

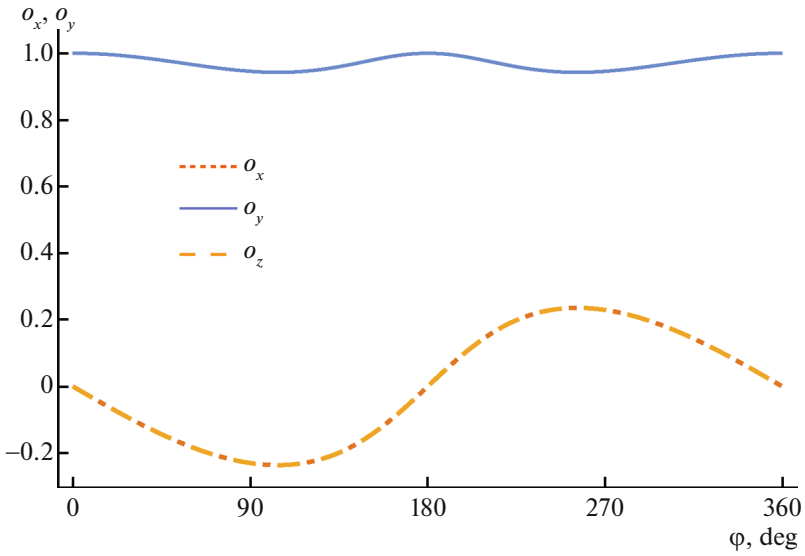

Fig. 5. The projections of the polarization vector $\mathbf{o}_s(\varphi, \alpha, \theta)$ in BBO crystal as a function of the polar angle φ calculated in the pump basis. Calculations were made for non-collinear ($\alpha = 13.6°$) frequency-degenerate regime with 800-nm pumping ($\theta = 45°$). The curves for horizontal components coincide.

4. ROLE OF THE POLARIZATION-ANGULAR SPECTRUM OF SPDC IN REDUCING THE ENTANGLEMENT OF QUANTUM STATES IN I-TYPE SPDC GENERATORS

Here we will consider a typical two-crystal scheme for obtaining polarization-entangled biphotons in an type-I SPDC-generator [6, 29]. The typical scheme is shown in Fig. 6. Two identical nonlinear crystals, which are cut under the first type of phase-matching, are located close to each other and are oriented orthogonally.

The pump beam, which is polarized at 45° to the horizontal direction, excites the both SPDC crystals in the non-collinear mode. The pump radiation is

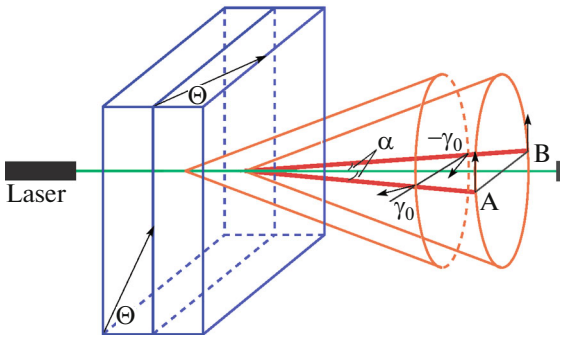

Fig. 6. The principle scheme of a double-crystal type-I SPDC generator. The arrows indicate the polarization directions of the SPDC radiation in both crystals taking the Migdall effect into account.

divided into ordinary and extraordinary polarized waves during propagation in nonlinear crystals. The extraordinary polarized waves pump the crystals and stimulate SPDC. The ordinary polarized waves pass through the crystals without meeting the conditions for phase-matching and, therefore, without scattering. Radiation that scattered in the crystals forms two almost coinciding cones.

In the most common experimental scheme (Fig. 6) SPDC radiation is collected from two diametrically opposed directions *OA* and *OB*. If we do not consider the dependence of polarization direction on polar angle, the state of the biphoton pairs at the output of this scheme can be written as

$$|\Psi_0\rangle = \frac{|HH\rangle + e^{i\delta}|VV\rangle}{\sqrt{2}}, \qquad (10)$$

where the basis vectors $|\mathrm{H}\rangle$ and $|\mathrm{V}\rangle$ have the conventional meaning, namely, the vector $|\mathrm{V}\rangle$ is perpendicular to the principal plane of the pump and the vector $|\mathrm{H}\rangle$ lies in this plane in the direction that is perpendicular to the SPDC beam. It is obvious that in general the Migdall effect reduces the degree of entanglement of the generated state and thereby decreases the "indicator" of entanglement. Indeed, due to the Migdall effect polarizations of signal and idler beams generated in the first crystal are rotated by the same (in absolute value) angle γ_0 but in the opposite directions. In contrast, polarization of signal and idler beams generated in the second crystal does not test the polarization rotation effect. It is easy to find the mathematical expression for the generated state by modification of the state (10). It is sufficient for this purpose to act on the *H*-polarized photon via a rotation matrix around the direction of the SPDC beam at the angle γ_0

$$\hat{S}(\gamma_0) = \begin{pmatrix} \cos\gamma_0 & \sin\gamma_0 \\ -\sin\gamma_0 & \cos\gamma_0 \end{pmatrix}. \qquad (11)$$

As a result we can get the following expression for the generated state:

$$|\Psi\rangle \propto \hat{S}(\gamma_0)|H\rangle \otimes \hat{S}(-\gamma_0)|H\rangle + e^{i\delta}|V\rangle \otimes |V\rangle. \qquad (12)$$

Using Fig. 2, it is not difficult to obtain the relationship between the angle γ_0 and the angle γ, which was introduced in the previous sections. In fact, in this two-crystal scheme the vertical component of wave electric field $|\mathbf{H}\rangle$ generated in the first crystal can be written in the pump basis as follows:

$$|\mathbf{H}\rangle = \{0, \cos\alpha, -\sin\alpha\}.$$

The angle γ_0 can be expressed through the scalar product of this vector and the vector $\mathbf{o}_s(\varphi, \alpha, \theta)$ taken for the angle $\pi/2$:

$$\gamma_0 = \arccos\left[\left(\mathbf{o}_s\left(\frac{\pi}{2}, \alpha, \theta\right)\cdot \mathbf{H}\right)\right]. \qquad (13)$$

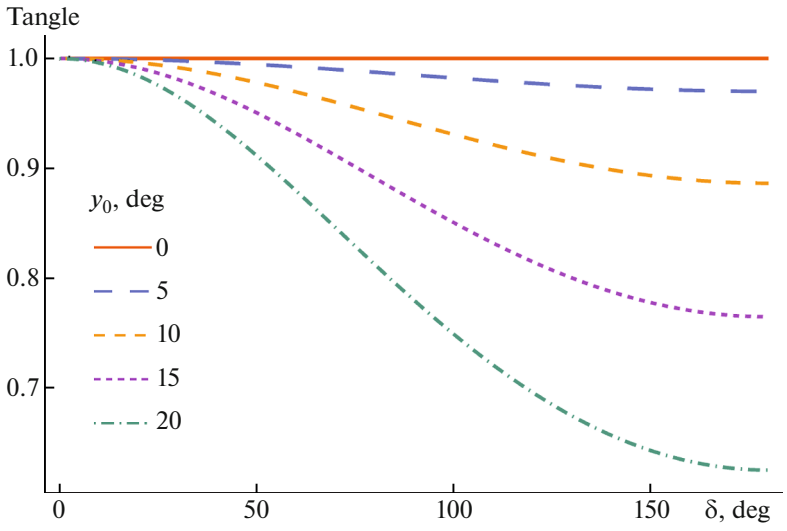

Fig. 7. The dependence of the entanglement of the state 12 on the phase δ at different angles γ_0.

The last expression shows that the angle γ_0 is a function of the angles (α, θ), whose explicit form is determined by formulas (6), (7) and (13).

One of the most commonly used characteristics of the entanglement of photons is the "Tangle" [29]. This characteristic takes the value 0 for a factorized state, while for a completely entangled state (for example Bell state) it is 1. For a pure state that corresponds to the case under consideration, the criterion of entanglement is introduced as follows. The entirely asymmetric transformation of the wave function $|\psi\rangle$ is carried out in $SU(2)$ algebra:

$$|\tilde{\psi}\rangle = \hat{\sigma}_2 \otimes \hat{\sigma}_2 |\psi^*\rangle, \quad (14)$$

where

$$\hat{\sigma}_2 = \begin{pmatrix} 0 & -i \\ i & 0 \end{pmatrix}$$

is the second of the Pauli matrices and (ψ^*) indicates complex conjugation. The Tangle is defined as the "closeness" of the state that is obtained by this transformation to the original:

$$T(\psi) = |\langle \psi | \tilde{\psi} \rangle|^2. \quad (15)$$

Figure 7 shows the curves obtained by calculating the Tangle according to the formula (15) taking into account the formulas (11), (12) and (14).

Two trends in deteriorating the entanglement of quantum states are clearly visible. Firstly, entanglement deteriorates with increasing the angle γ_0 and secondly, with an increase of the phase δ. It was found that the entanglement of this state has an interesting feature: if $\delta = 0$, it does not deteriorate. The maximum decrease in the entanglement occurs at $\delta = \pi$.

To understand the reason why there is no loss of entanglement when $\delta = 0$, we write down the explicit form of the condition (12) for $\delta = 0$:

$$|\Psi_{\delta=0}\rangle = \frac{1}{\sqrt{2}}(\hat{S}(\gamma_0)|H\rangle \otimes |H\rangle + \hat{S}(\gamma_0)|V\rangle \otimes |V\rangle), \quad (16)$$

which corresponds to the fact that the signal (idler) beam is "turned" as a whole by the angle γ_0 ($-\gamma_0$).

5. CONCLUSIONS

In this work we analyzed some manifestations of the Migdall effect, that lead to decreasing the entanglement of states of biphotons obtained in a standard double-crystal SPDC scheme. The results of a detailed analysis of the polarization-angular spectrum of type-I SPDC in uniaxial crystals made in the pump basis are also presented. It was shown that the tilt of the polarization vector in this basis is determined by the angle $\gamma(\alpha, \theta)$, which has a clear physical meaning of being the angle between the principal planes that belong to the pump beam and the selected SPDC beam.

We believe that these results may be useful for finding methods of full compensation of the Migdall effect. Solution of this problem provides an opportunity to create even more high-quality sources of entangled polarization photons based on SPDC.

6. ACKNOWLEDGMENTS

We thank Prof. A.S. Chirkin for continued interest in the work and for fruitful discussions, and Dr. I.E. Protsenko and Dr. M.Yu. Saygin for useful cooperation.

REFERENCES

1. D. N. Klyshko, in Proc. All-Union Meeting on Nonlinear Properties of Media, Chernogolovka, 1966.
2. D. N. Klyshko, JETP Lett. **6**, 23 (1967).
3. S. A. Akhmanov, B. B. Fadeev, R. V. Khokhlov, and O. H. Chunaev, Pis'ma Zh. Eksp. Teor. Fiz. **6**, 575 (1967).
4. S. E. Harris, M. K. Oshman, and R. L. Byer, Phys. Rev. Lett. **18**, 732 (1967).
5. N. Douglas and H. Mahr, Phys. Rev. Lett. **18**, 905 (1967).
6. P. G. Kwiat, E. Waks, A. G. White, I. Appelbaum, and P. H. Ebe rhard, Phys. Rev. A: Atom., Molec., Optic. Phys. **60**, R773 (1999).
7. F. Steinlechner, P. Trojek, M. Jofre, H. Weier, D. Perez, T. Jennewein, R. Ursin, J. Rarity, M. W. Mitchell, J. P. Torres, H. Weinfurter, and V. Pruneri, Opt. Express **20**, 9640 (2012).
8. R. Rangarajan, M. Goggin, and P. Kwiat, Opt. Express **17**, 18920 (2009).
9. T. G. Noh, H. Kim, Ch. J. Youn, S. B. Cho, J. Hong, T. Zyung, and J. Kim, Opt. Express **14**, 2805 (2006).
10. H. K. Lo, M. Curty, and K. Tamaki, Nature Photon. **8**, 595 (2014).
11. D. Bouwmeester, A. Ekert, and A. Zeilinger, The Physics of Quantum Information, (Springer-Verlag, 2000; Postmarket, Moscow, 2002).
12. Y. H. Kim, S. P. Kulik, and Y. Shih, Phys. Rev. Lett. **86**, 1370 (2001).
13. W. Pfaff, B. J. Hensen, H. Bemien, S. B. van Dam, M. S. Blok, T. H. Taminiau, M. J. Tiggelman, R. N. Schouten, M. Markham, D. J. Twitchen, and R. Hanson, Science **345**, 532 (2014).
14. K. Mattle, H. Weinfurter, P. G. Kwiat, and A. Zeilinger, Phys. Rev. Lett. **76**, 4656 (1996).
15. M. Schlosshauer, J. Kofter, and A. Zeilinger, Ann. Phys. **525**, A51 (2013).
16. M. P. van Exter, A. Aiello, S. S. R. Oemrawsingh, G. Nienhuis, and J. P. Woerdman, Phys. Rev. A: Atom., Molec., Optic. Phys. **74**, 012309 (2006).
17. S. Takeuchi, Japan. J. Appl. Phys. **53**, 030101 (2014).
18. R. Ramirez-Alarcon, H. Cruz-Ramirez, and A. B. U'ren, Laser Phys. **23**, 055204 (2013).

19. A. Migdall, J. Opt. Soc. Am. **14**, 1093 (1997).
20. R. Rangarajan, A. B. U'ren, and P. G. Kwiat, J. Modern Optics **58**, 312 (2011).
21. N. Boeuf, D. Branning, I. Chaperot, E. Dauler, S. Gue'rin, G. Jaeger, A. Muller, and A. Migdall, Opt. Eng. **39**, 1016 (2000).
22. S. Y. Baek and Y. H. Kim, Phys. Rev. A: Atom., Molec., Optic. Phys. **77**, 043807 (2008).
23. Y. X. Gong, P. Xu, J. Shi, L. Chen, X. Q. Yu, P. Xue, and S. N. Zhu, Opt. Lett. **37**, 4374 (2012).
24. C. A. Akhmanov and R. V. Khokhlov, Sov. Phys.-Usp. **9**, 210 (1966).
25. S. A. Magnitskiy, V. I. Malachova, A. P. Tarasevich, V. G. Tunkin, and S. D. Yakubovich, Opt. Lett. **11**, 18 (1986).
26. S. A. Magnitskiy, V. V. Firsov, N. M. Nagorskiy, I. Protsenko, and M. Saygin, in Laser Optics, 2014 International Conference (2014).
27. L. D. Landau and E. M. Lifshits, in Electrodynamics of Continuous Media, (Fizmatlit, Moscow,1959; Pergamon, Oxford, 1960).
28. K. Kato, IEEE J. Quantum Electron. **22**, 1013 (1986).
29. N. A. Peters and P. G. Kwiat, Phys. Rev. A: Atom., Molec., Optic. Phys. **70**, 052309 (2004).